Mid-infrared fiber-coupled QCL-QEPAS sensor

Vincenzo Spagnolo, Pietro Patimisco, Simone Borri, Gaetano Scamarcio, Bruce E. Bernacki & Jason Kriesel

Applied Physics B
Lasers and Optics

ISSN 0946-2171
Volume 112
Number 1

Appl. Phys. B (2013) 112:25-33
DOI 10.1007/s00340-013-5388-3

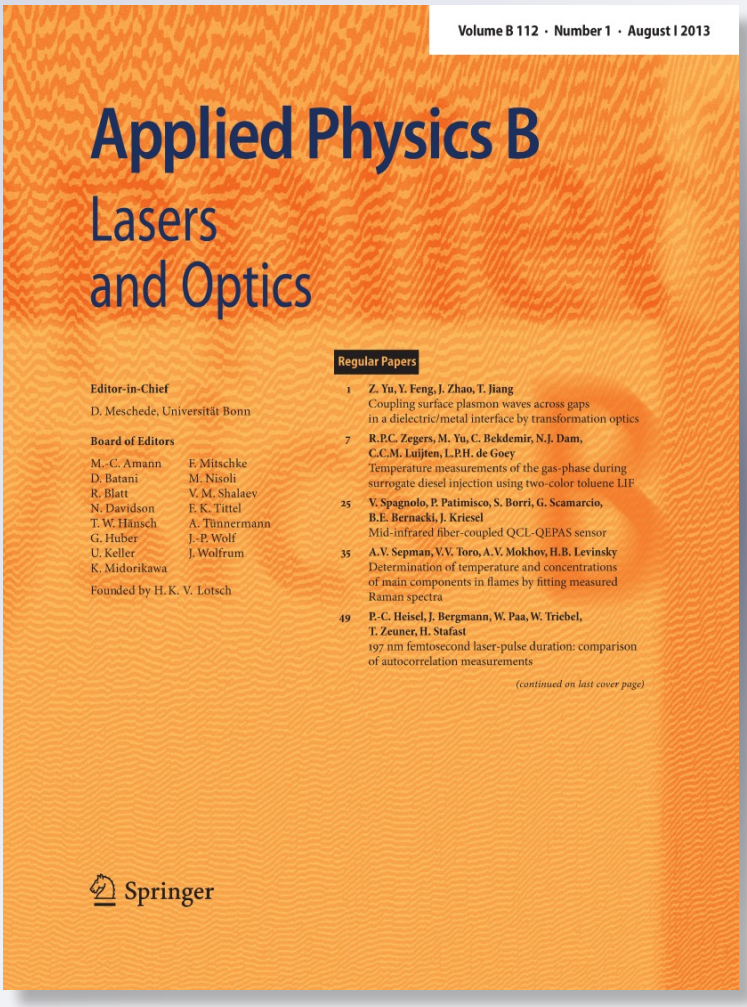

Springer

Appl. Phys. B (2013) 112:25–33
DOI 10.1007/s00340-013-5388-3

Applied Physics B
Lasers and Optics

Mid-infrared fiber-coupled QCL-QEPAS sensor

Vincenzo Spagnolo · Pietro Patimisco · Simone Borri · Gaetano Scamarcio · Bruce E. Bernacki · Jason Kriesel

Received: 17 December 2012 / Accepted: 20 February 2013 / Published online: 2 March 2013

Abstract An innovative spectroscopic system based on an external cavity quantum cascade laser (EC-QCL) coupled with a mid-infrared (mid-IR) fiber and quartz enhanced photoacoustic spectroscopy (QEPAS) is described. SF_6 has been selected as a target gas in demonstration of the system for trace gas sensing. Single mode laser delivery through the prongs of the quartz tuning fork has been obtained employing a hollow waveguide fiber with inner silver–silver iodine (Ag–AgI) coatings and internal core diameter of 300 μm. A detailed design and realization of the QCL fiber coupling and output collimator system allowed almost practically all (99.4 %) of the laser beam to be transmitted through the spectrophone module. The achieved sensitivity of the system is 50 parts per trillion in 1 s, corresponding to a record for QEPAS normalized noise-equivalent absorption of 2.7×10^{-10} W cm^{-1} Hz$^{-1/2}$.

1 Introduction

The development of compact optical sensors for trace chemical species in the gas phase is of interest for a large number of applications such as environmental monitoring, industrial process control and medical diagnostics. Laser absorption spectroscopic (LAS) techniques have been proved to be an extremely effective tool for the detection and quantification of molecular trace gases in the mid-infrared spectral region, and a significant improvement has been achieved with the advent of high performance quantum cascade lasers (QCLs) [1]. QCLs are unipolar laser based on electronic transitions between confined states created in the conduction band with the alternate growth of well and barrier materials. Their emission wavelengths can be tuned by design of the band structure. They can operate over a wide range of mid-infrared wavelengths from ~3 to ~24 μm and overcome some of the major drawbacks of other traditional mid-IR laser sources, i.e. lack of continuous wavelength tunability and large size and weight of gas lasers, large size and cooling requirement of lead salt diode lasers, complexity and low power of nonlinear optical sources. Continuous wave (CW) QCL devices capable of thermo-electrically cooled, room-temperature operation, single mode emission with mode-hop-free frequency tuning, high power (tens to hundreds of mW), and intrinsic narrow emission linewidth are commercially available in the ~4–12 μm spectral range. In combination with these laser sources, photoacoustic spectroscopy (PAS) offers the advantage of high sensitivity (part per billion (ppb) detection limits), large dynamic range, compact set-up, fast time-response and simple optical alignment [2], if compared with other spectroscopic detection schemes such as cavity-enhanced absorption spectroscopy, which can offer better performances but require more sophisticated equipments [3].

In PAS, pressure waves can be produced by the absorption of modulated laser radiation in gas samples at acoustic frequencies by the target trace-gas species. In the conventional PAS, the common approach to detect the

V. Spagnolo (✉) · P. Patimisco · S. Borri · G. Scamarcio
Dipartimento Interateneo di Fisica, University and Politecnico of Bari, CNR-IFN UOS BARI, Via Amendola 173, Bari, Italy
e-mail: spagnolo@fisica.uniba.it

B. E. Bernacki
Pacific Northwest National Laboratory, 902 Battelle Boulevard, Richland, WA, USA

J. Kriesel
Opto-Knowledge Systems Inc., 19805 Hamilton Ave, Torrance, CA, USA

acoustic signal utilizes an acoustic resonator filled with the gas and sensitive microphone [2]. The absorber gas is accumulated in the acoustic mode of the resonator for Q oscillation periods, where Q is the quality factor of the resonator. The signal is proportional to the effective integration time $t = Q/f$ where f is the resonant frequency. Most often the Q is in the range 40–200 and $f = 1{,}000$–$4{,}000$ Hz.

A novel approach to the photoacoustic detection of trace gas is to use a quartz tuning fork as an acoustic transducer. The key innovation of this method, named Quartz Enhanced Photoacoustic Spectroscopic (QEPAS) [4] is to invert the common PAS approach and accumulate the acoustic energy in a sharply resonant piezoelectric transducer with a very high quality factor ($Q > 10{,}000$). When the quartz tuning fork (QTF) is mechanically deformed, electrical charges are generated on its surface only when the two prongs move in opposite directions (anti-symmetric mode of vibration). In vacuum, a tuning fork typically resonate at 32,768 (2^{15}) Hz, which results in a high immunity of QEPAS devices to background acoustic noise as a consequence of the following behavior: (i) the ambient acoustic noise density approximately follows a $1/f$ dependence and is very low above 10 kHz; (ii) the acoustic wavelength in air is $\sim$1 cm at 32 kHz and is longer at lower frequencies. Therefore, the sound waves emanating from a distant source tend to apply a force in the same direction upon the two tuning fork prongs positioned at <1 mm distance. This does not excite the piezoelectrically active mode in which the two prongs move in opposite directions; (iii) the width of the tuning fork resonance at atmospheric pressure is $\sim$4 Hz, and only frequency components in this narrow spectral band can produce efficient excitation of the tuning fork vibration. A typical watch QTF can have a value of Q up to 100,000 in vacuum and $Q = 8{,}000$ or higher at normal atmospheric pressure. Therefore, the corresponding energy accumulation time at atmospheric pressure is of the order of few hundreds of ms, which is a noticeably longer time than any practical gas-filled resonator can provide. Very efficient QEPAS sensors have been demonstrated for trace detection of several chemical species, such as NH_3, NO, CO_2, N_2O, CO, CH_2O, H_2O isotope, etc. [1, 4–14], down to single ppb concentration.

We selected for our experiments sulfur hexafluoride (SF_6) as the target gas molecule. SF_6 is an extremely stable, invisible, non-hazardous, inert gas with unique physical and chemical properties that make it ideally suited for some specialized applications. Worldwide, the dominant uses of SF_6 are in gas-insulated equipment for electrical transmission and distribution systems and in blanketing or degassing of molten reactive metals, such as magnesium and aluminum. SF_6 has also been employed in leak detection systems since it is an inert gas. Atmospheric measurements reveal a clear and distinct increase of the global mean surface concentration of SF_6, from 0.6 ppt (part-per-trillion) at the beginning of 1978 to 4 ppt today, due to main sources located in the industrialized northern mid-latitudes that generate distinct vertical and meridional concentration gradients in the atmosphere. These features have made SF_6 one of the most attractive tracers for atmospheric transport and mixing studies. Although its atmospheric concentration is less than 0.1 % of that of the major greenhouse gas (CO_2), the Intergovernmental Panel on Climate Change (IPCC) has identified the SF_6 as having the highest global warming potential (GWP) of all known gases [15]. It is estimated that one kilogram of SF_6 is equivalent to between 22,500 and 24,900 kg of CO_2 in terms of the greenhouse effect. This is due to its strong absorbance in the infrared and to its long lifetime in the atmosphere (estimated to be as high as 3,200 years). Although legislation regulating its release to the atmosphere is yet to be initiated, some jurisdictions have already adopted voluntary agreements on monitoring its release.

Since SF_6 is an extremely efficient absorber of infrared radiation (around 10.5 μm) and characterized by a fast Vibrational-Translational (V-T) relaxation rate [16], very good photoacoustic signals can be obtained, once an accurate absorption line selection is accomplished and PAS systems with sensitivity down to few tens of ppt have been demonstrated [17].

Fiber-optic components show enhanced versatility with respect to bulk optics, mostly in terms of flexible beam guidance and compactness. Furthermore, fibers could also be deployed advantageously as modal wavefront filters, optical path delay length control or for multi-axial beam combining [18]. There are various fields of application for infrared fibers, each one requiring special fiber properties such as nulling interferometry [19], high precision imaging and spectroscopy [20]. Moreover, fiber optics is a key enabling technology needed to improve the robustness and effectiveness of specific detection and calibration systems.

Enhanced versatility of QEPAS sensor systems can be obtained via optical fiber delivery and coupling. Small size sensors with simple optical alignment have been realized employing fiber-coupled system (incorporating QTF, acoustic resonator, and pre-aligned fiber focuser) between near-IR laser source and QEPAS spectrophones [13, 21]. The feasibility to extend this approach also to mid-IR light sources will allow compact integration with QCLs. However, due to limited availability of mid-IR single mode fibers, the implementation of fiber-coupled based QCL sensors has only very recently been reported by us in ref. [22].

We will report here a detailed description on the design and realization of an innovative optoacoustic sensors based on a QCL laser source fiber-coupled via a single mode hollow waveguide with a QEPAS cell module.

2 QEPAS setup

In this work, a water-cooled CW EC-QCL (Daylight Solutions model 21106-MHF) operating at $\lambda = 10.54$ μm was employed as the spectroscopic light source. At a QCL chip temperature of 17 °C, this laser has a tuning range of 931–1,004 cm^{-1} and a specified mode hop free tuning range of 931–985 cm^{-1}, corresponding to 5 % of its center wavelength, with output powers up to 90 mW. Precise and continuous control of the laser wavelength can be performed by two methods. The frequency can be scanned over $\sim$0.6 cm^{-1} by applying a sinusoidal voltage ramp of 100 V peak-to-peak at 1 Hz to a piezoelectric translator attached to the diffraction grating element of the EC-QCL, while for higher frequency modulation, an internal bias tee allows external modulation of the QCL current to obtain 0.1 cm^{-1} peak to peak wavelength modulation at up to 2 MHz.

The QEPAS-based gas sensor architecture is depicted in Fig. 1. To enhance the QEPAS signal, and hence increase the trace gas detection sensitivity the quartz tuning fork (QTF) used in this work was coupled with an acoustic organ pipe type micro-resonator (MR). Metal tubes with a length of 4.00 mm each and inner diameter of 0.84 mm were mounted on both sides of the QTF with a gap spacing of 30 μm. We selected these MR sizes to enhance the QEPAS signal at low gas pressure (below 100 Torr) [21]. The QEPAS spectrophone (SPh), consisting of the QTF and the MR, is mounted inside a vacuum-thigh cell with ZnSe windows. The pressure and flow rate of the sample gas through the SPh are controlled and maintained at the optimum level using a pressure controller and flow meter (MKS Instruments Type 640). The flow of the gas mixture was set at a constant rate of 45 scc min^{-1}. The QCL beam is coupled to the SPh using a fiber. The detail on this optical system is reported in the next paper subsection. The laser beam exiting the SPh passes through an optical gas cell (length 10 cm) filled with a 0.1 % SF_6 in N_2 and subsequently is incident on an IR detector (VIGO model PVI-3TE-6). Wavelength locking function was performed using the 3*f* component of the detector output as the reference in a feedback algorithm.

Wavelength modulation (WM) technique was implemented by applying a sinusoidal modulation to the diode laser current at half of the QTF resonance frequency $f_0/2$ and detecting the QTF response at f_0 by means of a lock-in amplifier. Therefore, we performed WM QEPAS spectral measurements by slowly scanning the laser wavelength

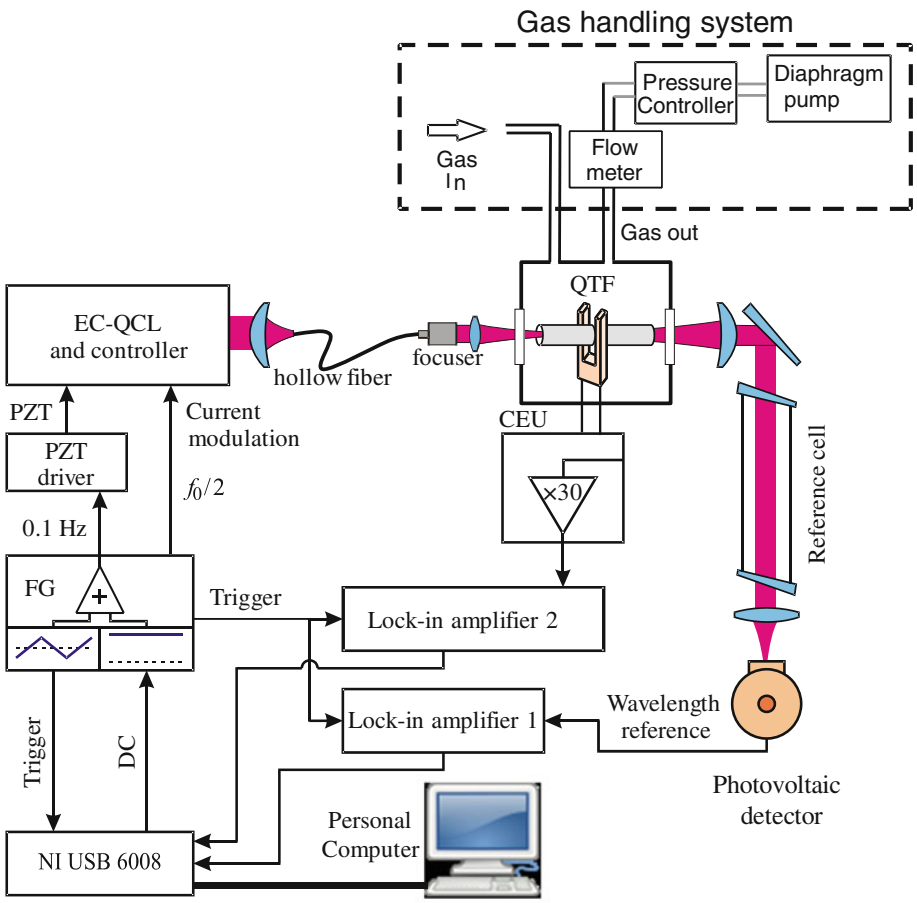

Fig. 1 Schematic of the fiber-coupled QEPAS sensor. *PZT* piezoelectric translator, *QTF* quartz tuning fork, *FG* dual channel function generator and *CEU* control electronics unit

using the piezoelectric translator (PZT). The piezoelectric signal generated by the QTF is amplified by a custom designed transimpedance amplifier (feedback resistor $R_{fb} = 10$ MΩ). Subsequently the signal is demodulated by a lock-in amplifier (Stanford Research Model SR830) and digitalized by a USB data acquisition card (National Instruments DAQCard USB6008), which is connected to a personal computer. The control electronic unit (CEU) allows the determination of the electromechanical parameters of the QTF: its dynamic resistance R, quality factor Q, and resonant frequency f_0. The physical parameters of the SPh at 75 Torr and using N_2 as gas carrier are $Q \sim 23{,}000$, $f_0 = 32{,}763$ Hz and $R = 54.7$ KΩ, from this data we can extract a QTF thermal noise of 6 μV [21]. The lock-in amplifiers and a function generator (Tektronix model AFG3102) are connected with an USB NI card. Data acquisition and recording is performed by a LabVIEW-based software. The time constant of the lock-in amplifiers was set to $\tau = 100$ ms for all QEPAS measurements reported in this work, this corresponds to a 0.16675 Hz bandwidth (12 dB/octave filter slope).

3 Single mode mid-IR fiber coupling system

In QEPAS experiments, it is critical to avoid laser illumination of the SPh system, since the radiation blocked by the MR tubes or by the QTF prongs results in an undesirable non-zero background. This background can be several times larger than the thermal noise level of QEPAS and carries a shifting fringe-like interference pattern, which limits the detection sensitivity [10, 23]. Thus, it is important to employ a mid-infrared QEPAS excitation beam of high quality and stability and if employing a fiber coupling system, single mode beam delivery is strictly required. Hollow waveguides have been demonstrated to be very efficient for mid-IR QCL beam single-mode delivery [24, 25].

Thus, we designed and assembled a fiber coupling system between the QEPAS SPh and the EC-QCL. Single mode laser delivery has been obtained by employing a hollow fiber with inner silver–silver iodine (Ag–AgI) coatings and an internal bore size of 300 μm, having a transmission loss of 1 dB/m and bending loss of 0.1 dB [20]. The basic structure of the fiber is shown in Fig. 2a. To fabricate a hollow fiber for mid-IR applications, an Ag layer is deposited inside the glass capillary tube by flowing a silver solution through the tube. Following this, a dielectric layer is formed by flowing an iodine solution that reacts with the silver to form AgI. By controlling the thickness of the AgI dielectric layer, the transmission window of the fiber can be optimized for a specific wavelength range from 2.5 to 18 μm, see Fig. 2b. While the relative spectral transmission is determined by the coating, the overall loss and spatial mode properties are governed by the bore size. The smaller the bore diameter (d) the better the mode properties, with single-mode (Gaussian beam profile) output when $d \leq 30\lambda$. However, for practical applications a small bore size is not always desirable, since the smaller the bore size, the greater the loss, scaling as $1/d^3$. For laser wavelengths near $\lambda \sim 10$ μm, a 300 μm bore fiber offers an appealing compromise by providing single-mode beam delivery with only moderate loss.

Both the laser fiber coupling and the fiber output focuser optics have been designed and realized in order to provide a focusing distance of 40 mm and produce a laser beam shaping so that the light coming out the collimator is transmitted through the SPh module without touching it.

The fiber optic sub-system consists of fiber coupling optics to couple EC-QCL output into the hollow core fiber (HCF), as well as optics to collimate the output of the HCF and focus the EC-QCL light between the tines of the tuning fork. To maximize coupling efficiency into the HCF, the output of the EC-QCL must be correctly mode-matched to

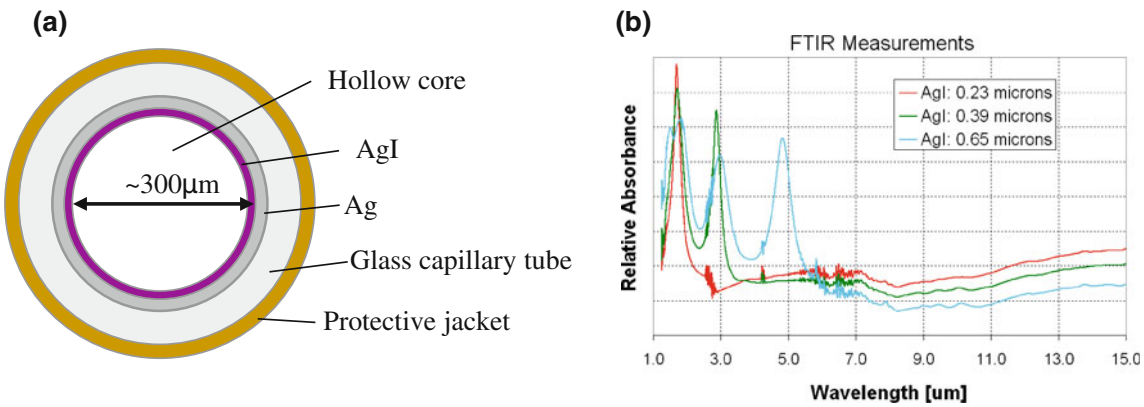

Fig. 2 **a** Simple schematic of hollow fiber with Ag/AgI coating (thickness not to scale). **b** FTIR relative absorbance measurements of fibers with different AgI coating thicknesses

optimally couple into the ~0.04 numerical aperture (NA) of the HCF. The more critical design concern is the correct lens choice for focusing the collimated output of the HCF to (1) ensure a spot diameter <300 μm to maximize the laser light delivered to the fork tines and analyte, and (2) to properly truncate the collimated Gaussian beam to reduce the side lobes of the focused spot in order to reduce thermal noise. The $1/e^2$ radius of the collimated fiber output is ~2.2 mm at 10.54 μm. A ZnSe lens with 12.7-mm diameter and 40-mm focal length was selected to meet the design criteria (Thorlabs LZ7673-F). The Gaussian intensity is reduced ~−70 dB at the edge of the lens aperture, which ensures good side lobe suppression. The resulting design was modeled using scalar diffraction calculations in ZEMAX, and the spot size at the entry to the resonator tube, along with an outline of the resonator tube, is shown in Fig. 3 where it can be seen that the spot diameter is much smaller than the resonator tube inner diameter. At the focal plane of the lens, the spot intensity falls −60 dB below the peak laser intensity, and this is shown in the log intensity plot of Fig. 4, where the suppressed side lobes are also apparent.

In Fig. 5, the 3D laser beam profile measured using a pyroelectric camera (mod. Spiricon Pyrocam III-C) 25 mm after exiting the fiber (Fig. 5a) and at the focusing plane of the collimator (Fig. 5b), with the corresponding one-dimensional profile on a log scale is shown. From a Gaussian fit of the focused beam profile (see Fig. 5b), we estimated a beam waist diameter of ~160 μm, well below the gap between the QTF prongs (~300 μm). As a result,

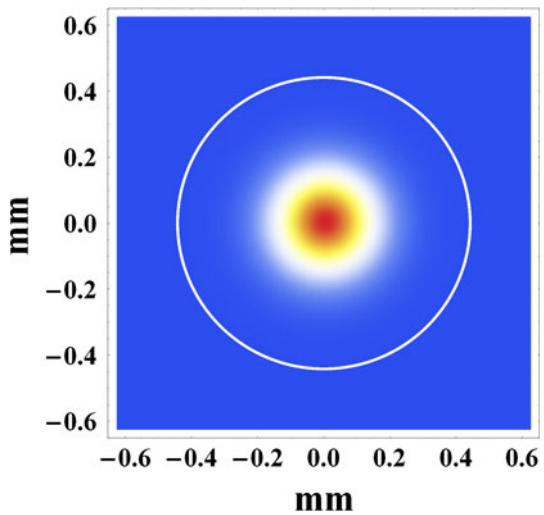

Fig. 3 Scalar diffraction calculation showing the intensity profile of the spot focused at the gap between the tuning fork tines. Also superimposed is the outline of the resonator tube's inner diameter showing the relative spot size with respect to the resonator tube aperture and large design margin to ensure efficient beam delivery to the analyte

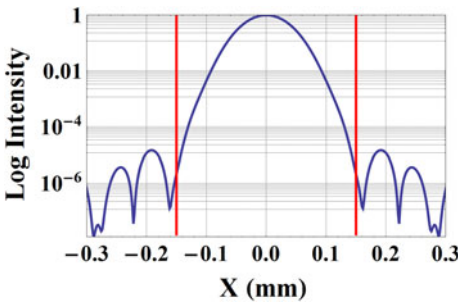

Fig. 4 Log intensity of the focused spot between the tuning fork tines showing the greatly suppressed side lobes −60 dB reduced in intensity compared to the peak intensity. The red vertical lines show the edges of the tuning fork tines

almost all (99.4 %) of the laser beam coming out the collimator were transmitted through the SPh module without touching it, thus strongly reducing the background fringe-like pattern in the QEPAS spectra.

4 Experimental results

According to the HITRAN database [26] the ν_3 fundamental band fundamental absorption band for SF_6 is peaked at 947.93 cm^{-1}. In Fig. 6, the simulated absorption spectra for a gas mixture of standard air and 10 ppm of SF_6 at 75 Torr pressure in the range 947–950 cm^{-1}, using HITRAN database is shown. At ~948.26 cm^{-1} a peak due to water vapor is clearly visible, so we have to select a SF_6 absorption line far enough from it to not suffer interference effects. No other spectral features apart from those belonging to SF_6 are visible. Thus, for our QEPAS experiment we selected the spectral range 948.4–949 cm^{-1}, since in this range the SF_6 absorption lines show the lowest background absorption signal.

A trace gas standard generator is used to produce SF_6 concentrations in the range 0–160 ppb, using pure or humidified N_2 as the diluting gas, starting from a certified 10 ppm SF_6 in N_2 mixture. We use a Nafion humidifier (PermaPure) to add water vapor to the gas samples. A needle valve was employed to set the gas flow to a constant rate of 100 scc min^{-1}. To select the best SF_6 spectral line in terms of absorption strength and absence of interference effects from other gases, we made a comparison between the absorption spectra measured using the reference cell filled with 0.1 % SF_6 in N_2 and the QEPAS signal obtained in amplitude modulation spectroscopy configuration for a SF_6 concentration of 160 ppb in humidified N_2. The results are shown in Fig. 7, in both cases the gas pressure was set to 75 Torr.

Based on the obtained data, we select for our experiments the SF_6 absorption line located at 948.615 cm^{-1}, since it gives a high QEPAS signal and is far enough from

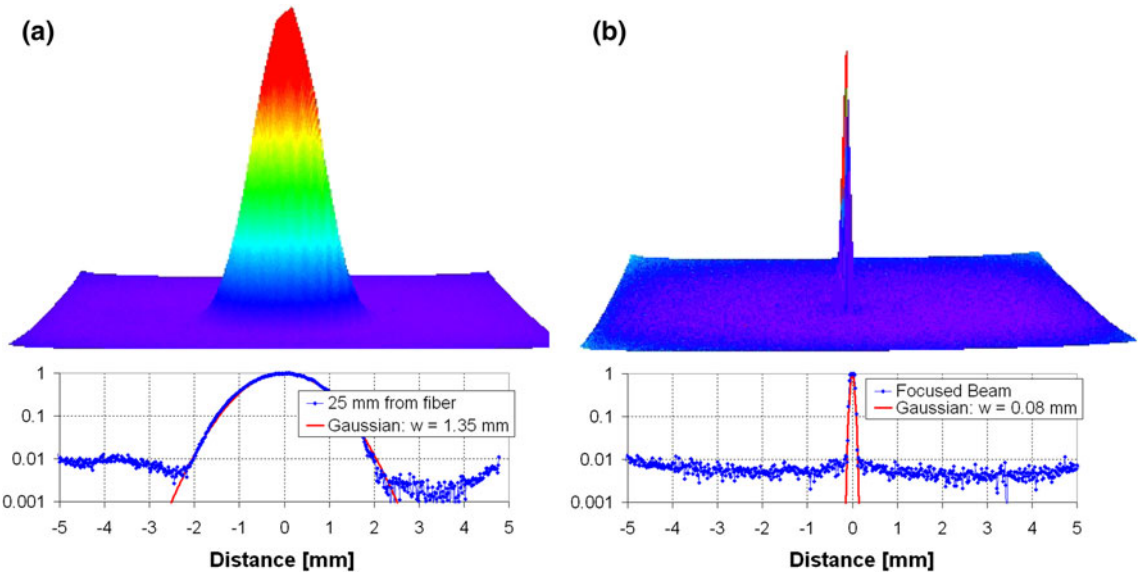

Fig. 5 **a** Three-dimensional single mode profile of the EC-QCL beam measured 25 mm after exiting the fiber. **b** Three-dimensional single mode profile of the EC-QCL beam at the focal point of the focusing assembly. In both panels, the corresponding one-dimensional profile on a log scale and the related Gaussian fit is also shown

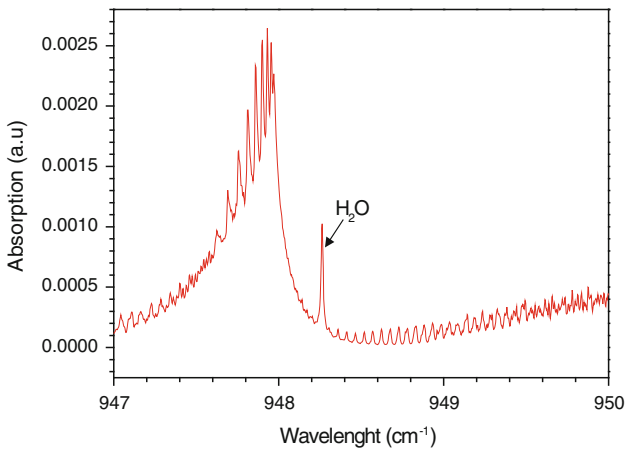

Fig. 6 HITRAN simulation of the absorption spectra calculated for a gas mixture of 0.1 % of SF_6 in standard air at 75 Torr pressure. The peak at $\sim$948.2 cm^{-1} is due to water vapor; all the other spectral features are due to SF_6

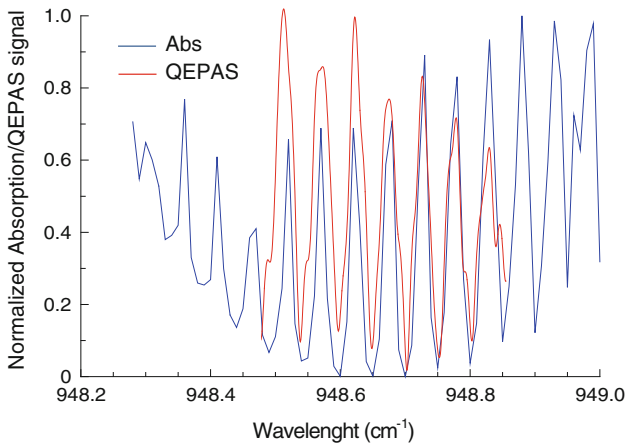

Fig. 7 Comparison between the absorption spectra measured for a gas mixture of 0.1 % of SF_6 in N_2 and the QEPAS signal measured for a gas mixture of 160 ppb of SF_6 in humidified N_2, both at 75 Torr pressure

water lines. This last statement was verified by comparing the spectra obtained for SF_6:N_2 mixture having the same SF_6 concentration with or without adding water vapor.

For the selected SF_6 absorption line (948.615 cm^{-1}) the optical power emitted by the EC-QCL is 28 mW. In our QEPAS experiments we implemented a 1 m long hollow fiber. As a result, 65 % of the optical power emitted by the EC-QCLs is focused on the SPh module ($\sim$18 mW) and almost all (99.4 %) is transmitted through, without touching it. The 35 % optical power reduction is due mostly to fiber losses ($\sim$25 %) and partially to the focusing and collimating optics ($\sim$10 %). If we substitute the fiber coupling system with a "standard" pinhole + lens optical system (we used a 25.4-mm diameter ZnSe lens with a focusing length of 38 mm), 80 % of the laser optical power ($\sim$22.5 mW) reached the SPh.

To find the optimal operating condition in terms of QEPAS signal-to-noise ratio, we investigated the effects of gas pressure and WM amplitude. The gas pressure influences the QEPAS signal since (i) the *Q*-factor decreases at higher pressures, (ii) the peak optical absorption varies with pressure, (iii) the V-T energy transfer relaxation rate from vibrational to translational degrees of freedom is faster at higher pressures, resulting in more efficient sound

excitation and the acoustic resonator enhancement factor changes with pressure [4]. Great care must also be taken to optimize the laser wavelength modulation amplitude $\Delta\lambda$. The WM signal increases by decreasing the gas mixing pressure due to line absorption narrowing.

Thus, in the investigated gas pressure range from 50 to 760 Torr we performed WM experiments modulating the laser current by applying a sinusoidal voltage signal to the laser driver in the range of 1.5–5 V. The optimal sensor operating conditions were found to occur at a gas pressure of 75 Torr and a modulation amplitude $\Delta\lambda$ of 4.2 V. The QEPAS signal measured under these operating conditions is shown in Fig. 8, where the influence of the wavelength modulation on the QEPAS signal for a gas mixture containing 160 ppb of SF_6 in N_2, at 75 Torr pressure is reported. Note that the possibility to use low gas pressure is also advantageous since it allows us to isolate the selected SF_6 absorption band from the very near ($\sim$0.05 cm^{-1}) adjacent ones.

High-resolution WM QEPAS scans of a SF_6:N_2 humidified calibrated mixtures with different concentrations are shown in Fig. 9. No fringe-like interference pattern was observed, which is the result of using the fiber optical coupling system. The lack of clear zero signal off the SF_6 feature in Fig. 9 is due to the presence of neighboring SF_6 absorption lines. Note that at larger SF_6 concentration the QEPAS signal saturated the lock-in amplifier.

The small modulations observed in Fig. 9 for pure N_2 are mainly due to the minor portion (less than 1 %) of the laser light touching the SPh system. This baseline is reproducible so in principle it can be eliminated by post processing of the spectra, thus improving the resolution, but also increasing the overall measuring time.

In Fig. 10 a comparison between the QEPAS scan measured at the same gas mixture concentration (19 ppb of SF_6:N_2) using the fiber-coupled sensor and the QEPAS sensor employing standard optical system (pinhole + lens) is shown. In this last case, we measured a QEPAS peak signal of $\sim$125 mV, thus scaling with the laser optical power with respect to the fiber-coupled one (100 mV), although a small fringe-like interference pattern is clearly visible, proving that a non-negligible portion of the optical power is hitting the SPh. Considering the noise fluctuations $\sim$4 mV (see Fig. 9) and the QEPAS signal for 19 ppb $\sim$100 mV, we can extract for our fiber coupled QEPAS sensor a 1σ detection limit of $\sim$750 ppt, at 100 ms integration time. The corresponding detection limit for the standard optical system is $\sim$900 ppt, since to a 25 % higher QEPAS signal, corresponds a 50 % higher noise fluctuation (6 mV).

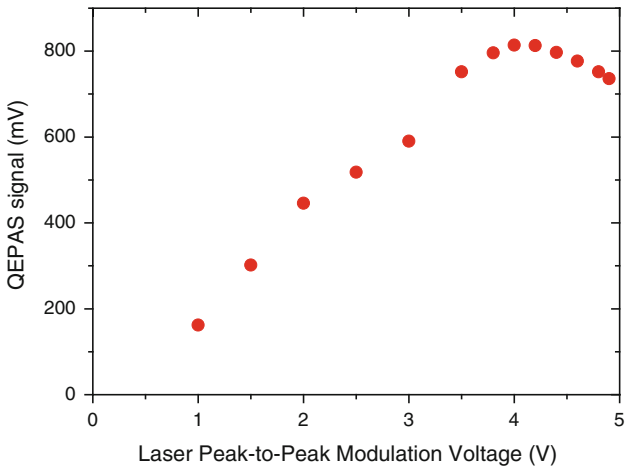

Fig. 8 QEPAS signal amplitude measured for 160 ppb SF_6 concentration in N_2 plotted at 75 Torr as a function of the QCL modulation voltage

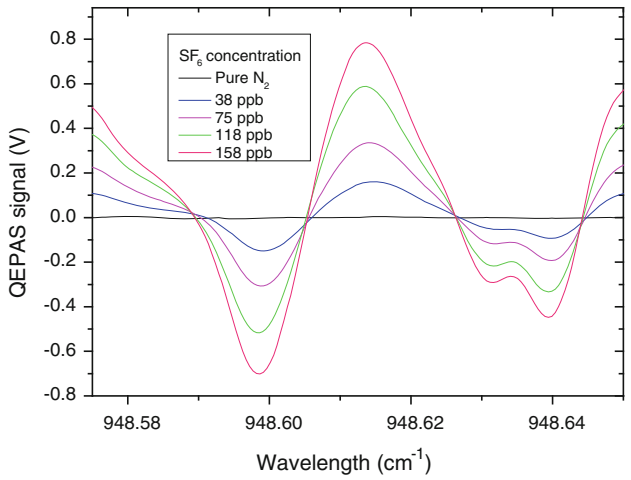

Fig. 9 Second-harmonic high-resolution QEPAS scans of SF_6:N_2 humidified calibrated mixtures with different SF_6 concentrations. The QEPAS cell pressure was set to 75 Torr

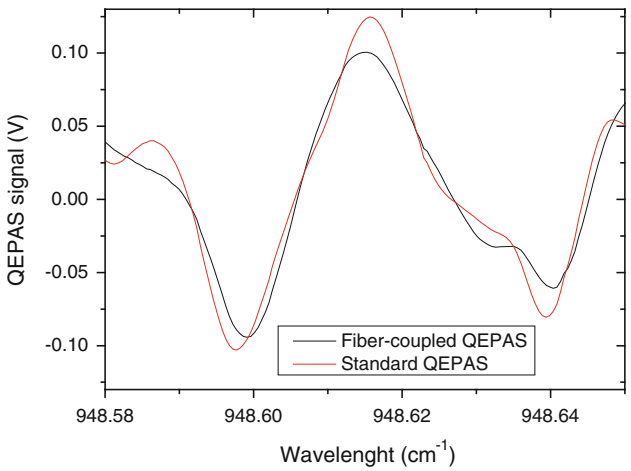

Fig. 10 Comparison between the QEPAS spectra measure for a 19 ppb SF_6 concentration in N_2 using the fiber-coupling system and the "standard" pinhole + lens optical system, between the QCL and the SPh

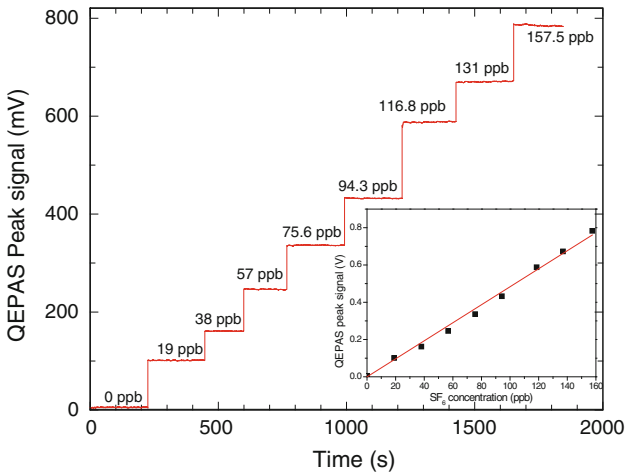

Fig. 11 Measured SF_6 concentrations obtained by varying settings of the trace gas standard generator. Inset: calibration curve obtained from measured QEPAS signals and corresponding SF_6 concentrations using gas mixture generator

Stepwise concentration measurements were performed to verify the linearity of the QEPAS signal as a function of the SF_6 concentration, with the system operating in the locked mode, i.e. with the EC-QCL frequency set to the center of the selected SF_6 absorption line. The QEPAS signal for each concentration step was measured every 100 ms, for a total time duration of more than 30 min. In order to allow the gas mixture concentration to stabilize, we stopped the QEPAS signal acquisition for 10 s when we change the SF_6 concentration. The results are shown in Fig. 11. Data for each step were averaged and a calibration curve was obtained (inset of Fig. 11) using the SF_6 concentrations derived from the gas standard generator. The results confirm that the QEPAS signal is proportional to the SF_6 concentration.

To determine the best achievable sensitivity of the QEPAS sensor we performed an Allan variance analysis [27], measuring and averaging the QEPAS signal [22]. For a 1 s averaging time we extract a minimum detection sensitivity of 50 parts per trillion (ppt), corresponding to a normalized noise equivalent absorption coefficient of NNEA = 2.7 × 10–10 cm^{-1} W $Hz^{-½}$, which represents a record value for the QEPAS technique [22]. The estimated QEPAS signal at 50 ppt concentration (~250 μV) is still several times larger than the QTF thermal noise (6 μV), meaning that the sensor detection is mostly limited by stability of the laser source and the small scattered light (~0.06 % of the total power) hitting the SPh structural elements.

5 Conclusions

In summary, the feasibility of an innovative spectroscopic system based on an external cavity quantum cascade laser (QCL) coupled with a mid-IR fiber and quartz enhanced photoacoustic spectroscopy was demonstrated. An hollow waveguide fiber with internal core diameter of 300 μm has allowed the QCL single mode beam delivery. We designed and realized an output collimator system able to transmit the fiber output beam through the spectrophone module without touching it. This allows us to strongly reduce signal interference patterns and, also taking advantage from the very fast V-T relaxation rate and the strong absorption strength of SF_6, to achieve a record QEPAS sensitivity in the ppt concentration range.

Acknowledgments The authors acknowledge financial support from the Italian research projects: PON01_02238 and PON02_00675.

References

1. R.F. Curl, F. Capasso, C. Gmachl, A.A. Kosterev, B. McManus, R. Lewicki, M. Pusharsky, G. Wysocki, F.K. Tittel, Quantum cascade lasers in chemical physics. Chem. Phys. Lett. **487**, 1–18 (2010)
2. A. Elia, P.M. Lugarà, C. Di Franco, V. Spagnolo, Photoacoustic techniques for trace gas sensing based on semiconductor laser sources. Sensors **9**, 9616–9628 (2009)
3. I. Galli, S. Bartalini, S. Borri, P. Cancio, D. Mazzotti, P. De Natale, G. Giusfredi, Molecular gas sensing below parts per trillion: radiocarbon-dioxide optical detection. Phys. Rev. Lett. **107**, 270802 (2011)
4. A.A. Kosterev, F.K. Tittel, D.V. Serebryakov, A.L. Malinovsky, I.V. Morozov, Applications of quartz tuning forks in spectroscopic gas sensing. Rev. Sci. Instrum. **76**, 043105 (2005)
5. A.A. Kosterev, Y.A. Bakhirkin, F.K. Tittel, Ultrasensitive gas detection by quartz-enhanced photoacoustic spectroscopy in the fundamental molecular absorption bands region. Appl. Phys. B **80**, 133–138 (2005)
6. R. Lewicki, G. Wysocki, A.A. Kosterev, F.K. Tittel, QEPAS based detection of broadband absorbing molecules using a widely tunable, cw quantum cascade laser at 8.4 μm. Opt. Express **15**, 7357–7366 (2007)
7. A.A. Kosterev, P.R. Buerki, L. Dong, M. Reed, T. Day, F.K. Tittel, QEPAS detector for rapid spectral measurements. Appl. Phys. B **100**, 173–180 (2010)
8. C. Bauer, U. Willer, W. Schade, Use of quantum cascade laser for detection of explosives: progress and challenges. Opt. Eng. **49**, 111126 (2010)
9. K. Liu, H. Yi, A.A. Kosterev, W. Chen, L. Dong, L. Wang, T. Tan, W. Zhang, F.K. Tittel, X. Gao, Trace gas detection based on off-beam quartz enhanced photoacoustic spectroscopy: optimization and performance evaluation. Rev. Sci. Inst. **81**, 103103 (2010)
10. L. Dong, V. Spagnolo, R. Lewicki, F.K. Tittel, Ppb-level detection of nitric oxide using an external cavity quantum cascade laser based QEPAS sensor. Opt. Express **19**, 24037–24045 (2011)
11. L. Dong, R. Lewicki, K. Liu, P.R. Buerki, M.J. Weida, F.K. Tittel, Ultra-sensitive carbon monoxide detection by using EC-QCL based quartz-enhanced photoacoustic spectroscopy. Appl. Phys. B **107**, 275–283 (2012)
12. V. Spagnolo, L. Dong, A.A. Kosterev, F.K. Tittel, Modulation cancellation method for isotope $^{18}O/^{16}O$ ratio measurements in water. Opt. Express **20**, 3401–3407 (2012)

13. S. Schilt, A.A. Kosterev, F.K. Tittel, Performance evaluation of a near infrared QEPAS based ethylene sensor. Appl. Phys. B **95**, 813–824 (2009)
14. M. C. Phillips, T. L. Myers, M. D. Wojcik, B. D. Cannon, "External cavity quantum cascade laser for quartz tuning fork photoacoustic spectroscopy of broad absorption features"
15. Intergovernmental Panel on Climate Change (IPCC), Climate Change 1994, Radiative Forcing of Climate Change. The Press Syndicate of the University of Cambridge. New York, NY (1994)
16. R.D. Bates Jr, J.T. Knudtson, G.W. Flynn, Energy transfer among excited vibrational states of SF_6. Chem. Phys. Lett. **8**, 103 (1971)
17. M.A. Gondal, A. Dastageer, M.H. Shwehdi, Photoacoustic spectrometry for trace gas analysis and leak detection using different cell geometries. Talanta **62**, 131–141 (2004)
18. A. Ksendzov, O. Lay, S. Martin, J.S: Sanghera, L.E: Busse, W.H. Kim, P.C. Pureza, V.Q. Nguyen, I.D. Aggarwal, Characterization of mid-infrared single mode fibers as modal filters, Appl. Opt. 46, 7957–7962 (2007)
19. A. Ksendzov, T. Lewi, O.P. Lay, S.R. Martin, R.O. Gappinger, P.R. Lawson, R.D. Peters, S. Shalem, A. Tsun, A. Katzir, Modal filtering for midinfrared nulling interferometry using single mode silver halide fibers. Appl. Opt. **47**, 5728–5735 (2008)
20. J.M. Kriesel, N. Gat, B.E. Bernacki, R.L. Erikson, B.D. Cannon, T.L. Myers, C.M. Bledt, J.A. Harrington, "Hollow core fiber optics for mid-wave and long-wave infrared spectroscopy", Proc. SPIE 8018, 80180V1-10 (2011)
21. L. Dong, A.A. Kosterev, D. Thomazy, F.K. Tittel, QEPAS spectrophones: design, optimization, and performance. Appl. Phys. B **100**, 627–635 (2010)
22. V. Spagnolo, P. Patimisco, S. Borri, G. Scamarcio, B.E. Bernacki, J. Kriesel, Part-per-trillion level SF6 detection using a quartz enhanced photoacoustic spectroscopy based sensor with single-mode fiber-coupled quantum cascade laser excitation. Optic Letters **37**, 460–462 (2012)
23. V. Spagnolo, A.A. Kosterev, L. Dong, R. Lewicki, F.K. Tittel, NO trace gas sensor based on quartz enhanced photoacoustic spectroscopy and external cavity quantum cascade laser. Appl. Phys. B **100**, 125–130 (2010)
24. J.A. Harrington, "Infrared Fibers and their applications", SPIE Press monograph (2004)
25. P. Patimisco, V. Spagnolo, M.S. Vitiello, A. Tredicucci, G. Scamarcio, C.M. Bledt, J.A. Harrington, Coupling external cavity mid-IR quantum cascade lasers with low loss hollow metallic/dielectric waveguides. Appl. Phys. B **102**, 255–260 (2012)
26. Available online: http://www.hitran.com
27. P. Werle, Accuracy and precision of laser spectrometers for trace gas sensing in the presence of optical fringes and atmospheric turbulence. Appl. Phys. B **102**, 313–329 (2011)